Research paper

Mixed hydrothermal and meteoric fluids evidenced by unusual H- and O-isotope compositions of kaolinite-halloysite in the Fe(-Mn) Tamra deposit (Nefza district, NW Tunisia)

Augustin Dekoninck[a,*], Béchir Moussi[b], Torsten Vennemann[c], Fakher Jamoussi[b], Nadine Mattielli[d], Sophie Decrée[e], Hédi-Ridha Chaftar[f], Nouri Hatira[f], Johan Yans[a]

[a] University of Namur, Institute of Life-Earth-Environment (ILEE), 61 rue de Bruxelles, B-5000, Namur, Belgium
[b] Centre de Recherche et des Technologies des Eaux (CERTE), Technopôle de Borj-Cédria, route touristique de Soliman, BP 273-8020, Soliman, Tunisia
[c] Université de Lausanne, Institut des Sciences de la Terre (ISTE), quartier UNIL-Mouline, bâtiment Géopolis, CH-1015 Lausanne, Switzerland
[d] Université Libre de Bruxelles, ULB, Laboratoire G-Time, DGES, 50 avenue F.D. Roosevelt, B-1050 Bruxelles, Belgium
[e] Royal Belgium Institute of Natural Sciences, rue Vautier 29, B-1000 Bruxelles, Belgium
[f] Office National des Mines, 24 rue 8601-2035, La Charguia I, Tunis, Tunisia

ARTICLE INFO

ABSTRACT

The iron mine of Tamra (Nefza District, NW Tunisia) is a 50 m thick Upper Mio-Pliocene sedimentary series impregnated by Fe-Mn oxides associated with white clay lenses with high halloysite and kaolinite content. This mineralization results from i) synsedimentary weathering/pedogenesis, and ii) mixing surface water and regional hydrothermal fluids. The oxygen and hydrogen isotope composition of halloysite-kaolinite and goethite-hematite is examined in order to provide new insights into the ore formation. This study concludes that halloysite-kaolinite was not equilibrated only with meteoric fluids: the $\delta^{18}O$ values have a range towards high values that are not consistent with weathering conditions for their formation and/or during their subsequent alteration. The δD and $\delta^{18}O$ values of goethite lead to the same conclusion. The stable isotope compositions could be related to fluid-rock interaction with the underlying marls (and/or skarns), providing relatively high $\delta^{18}O$ values to the fluids responsible for the white clay formation. This model also shows that the Pb-isotope compositions of halloysite-kaolinite are explained by a felsic and a carbonated end-member, similar to other ore deposits (IOCG and Sedex) of the vicinity. Several factors should be considered for the precipitation of halloysite-kaolinite and/or destabilization of primary clays in the Tamra ore, i.e. mixing of deep hot saline fluids, related to a thermally driven circulation, and meteoric waters. This hydrothermal contribution postdates the main synsedimentary weathering/pedogenetic Fe-enrichment and may be related to late Fe, Mn, Pb, Zn and As inputs of the Fe-Mn oxides.

1. Introduction

In the weathering environment, the isotopic composition of hydrogen and oxygen in water is related to the climatic conditions (Savin and Epstein, 1970). Some authigenic clay minerals and goethite are known to crystallize in isotopic equilibrium with meteoric water and, once crystallized, are resistant to isotopic exchange under the near surface conditions thanks to the slow isotopic exchange at low temperature (Yapp, 1990; Sheppard and Gilg, 1996; Savin and Hsieh, 1998). Sheppard and Gilg (1996) showed that oxygen and hydrogen composition of present-day kaolinite formed from meteoric water is largely temperature dependent and aligned along the "kaolinite line",

which is parallel to the meteoric water line. Yapp (1990) drew the same conclusion for supergene goethite. Therefore, any process (diagenesis, evaporation, hydrothermalism…) which do not equilibrate goethite and kaolinite with meteoric waters would record a shift in the oxygen and hydrogen isotope composition. In natural systems, processes of fluid/rock interactions could lead to isotopic exchange between a mineralizing fluid and bedrocks for example, but also between a matrix progressively infiltrated by external fluids in an open system (Savin and Lee, 1988). Dissolution-precipitation of minerals could change the isotopic composition of the fluid (weathering, hydrothermal, diagenetic). This is especially the case for oxygen, given its availability in most of the common minerals (i.e. silicates, oxides, and carbonates)

---

* Corresponding author.
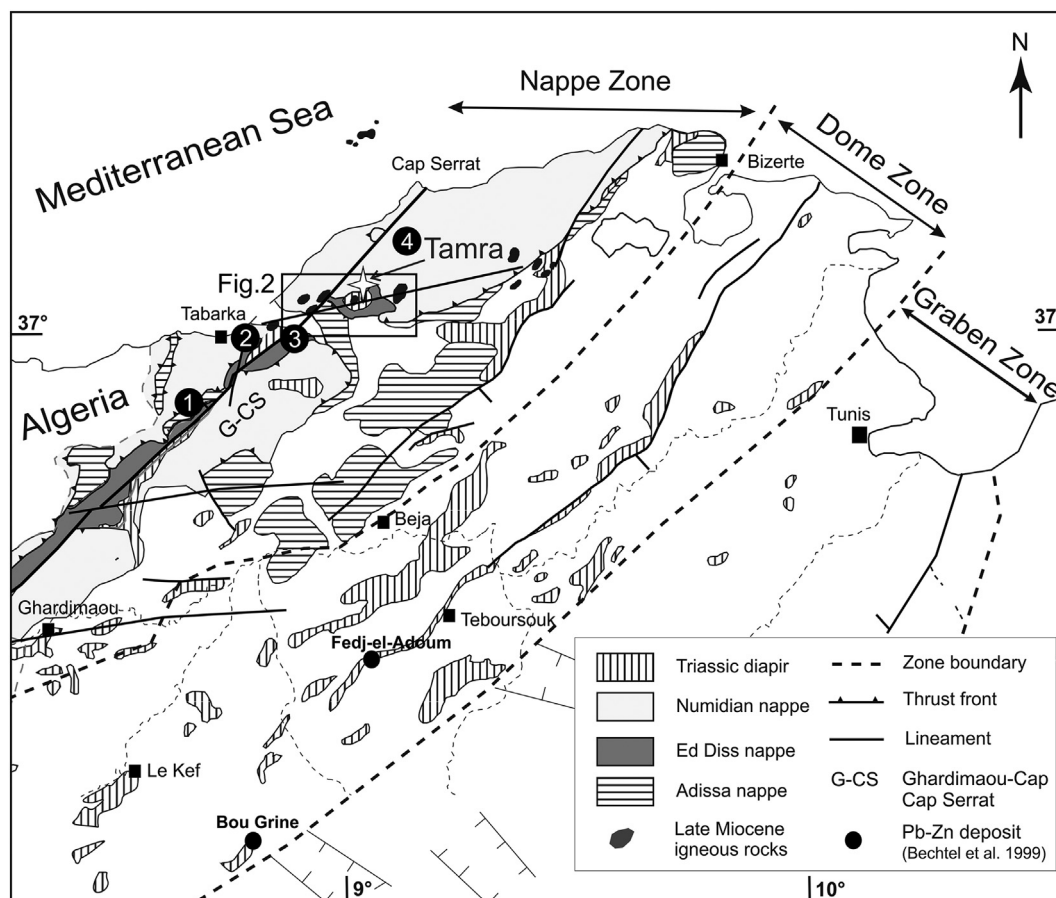*E-mail address:* augustin.dekoninck@unamur.be (A. Dekoninck).

Fig. 1. Tectonic map of central and northern Tunisia showing the location of the Nefza area (Fig. 2) and the Bou Grine and Fedj-el-Adoun Pb-Zn deposits. Numbers refer to sampling site: 1-Ain Drahan (14AD01), 2-Sidi Bader (14SB01, 14SB02), 3-Ain Sebaa (14ME02), 4-Om-Tébal (OMS2; modified after Rouvier et al., 1985; Bouaziz et al., 2002; Bouhlel et al., 2013; Decrée et al., 2016).

compared to hydrogen (hydroxides, hydrous silicates). For example, carbonates concentrate ^{18}O in their structure in contrast to other minerals (Garlick, 1966; Taylor, 1968; Kohn and Valley, 1998a, b, c; Hoefs, 2009), and when dissolved, release heavy oxygen to the fluids, which are depleted in ^{18}O (meteoric fluids). However, the range of these modifications depends on the isotopic fractionation, on the initial difference in isotopic composition between the fluid and the mineral, and on the temperature between the mineralizing fluid and minerals (Girard and Fouillac, 1995).

The Nefza mining district (NW Tunisia) illustrates well the complexity of mixing fluids and their interaction with volcanic and sedimentary rocks during the genesis of various types of deposits (Figs. 1 and 2; Decrée et al., 2008a, 2013, 2014, 2016; Moussi et al., 2011). The area has successively been affected by Serravalian to Tortonian felsic magmatism, which is responsible for contact metamorphism of Late Cretaceous to Eocene marls into skarn (Decrée et al., 2014), and also for the setting up of a Miocene Fe-Cu-Au-(U-REE) volcanic breccia around a Triassic diapiric dome (Decrée et al., 2013). The extensional conditions allowed the generation of Tortonian to Messinian basaltic flows and the deposition of two Late Miocene to Pliocene continental (siliciclastic and carbonate) deposits containing the Sidi Driss SEDEX Pb-Zn (Sidi Driss) and the Tamra Fe(-Mn) deposits (Decrée et al., 2008a, b, 2010). The synsedimentary weathering/pedogenesis through the 50 m thick Tamra sediments and the later hydrothermal circulation have led to enrichment in Fe and other elements in the sediments (Decrée et al., 2008b, 2010). Local concentration of "white clays" composed of kaolinite and halloysite is associated with the Fe-oxide ore (Moussi et al., 2011), and is considered to determine both meteoric and hydrothermal contributions. Therefore, hydrogen and oxygen isotope analyzes of the white

clays, associated with iron oxides and hydroxides, may help to redefine the process, which took place during mineralization in the Nefza mining district, taking into account the complexity and relationships of the rock varieties.

2. Geological settings

2.1. Geological framework

The Tamra Fe-Mn deposit is located in the Nefza mining district (NW of Tunisia, Fig. 1), which has been well-known for its base-metal deposits since the first half of the 20th century (Gottis and Sainfeld, 1952). The Nefza district is located in the Tellian "Nappe Zone" of Northern Tunisia, which is characterized by the Ed Diss Upper Cretaceous to Eocene thrust sheets (Burollet, 1991; Rouvier, 1994; Ould Bagga et al., 2006), and the overlying Oligocene "Numidian Nappe" (Fig. 1, Rouvier, 1977). Carbonates and marls from the Ed Diss sheet (Negra, 1987) are overlain by the "Numidian Nappe", which is composed of claystones and sandstones Oligocene to Burdigalian in age. Serravalian to Late Tortonian felsic magmatism (12.9 ± 0.5 Ma to 8.2 ± 0.4 Ma; Badgasarian, 1972; Bellon, 1976; Rouvier, 1977; Faul and Foland, 1980; Decrée et al., 2013) resulted in the emplacement of granodiorite and volcanic rhyodacite (Mauduit, 1978; Rouvier, 1994; Savelli, 2002; Decrée et al., 2014). Skarn deposits were formed in contact with late Cretaceous-Eocene marls (Fig. 2; Decrée et al., 2013). The most prominent feature of the area is the 7 km long and 3 km wide Oued Belif ring-shaped structure (Rouvier, 1987), characterized by a Fe-rich breccia containing reworked fragments of the regional substrates, and a small amount of volcanic-related material (Decrée et al.,
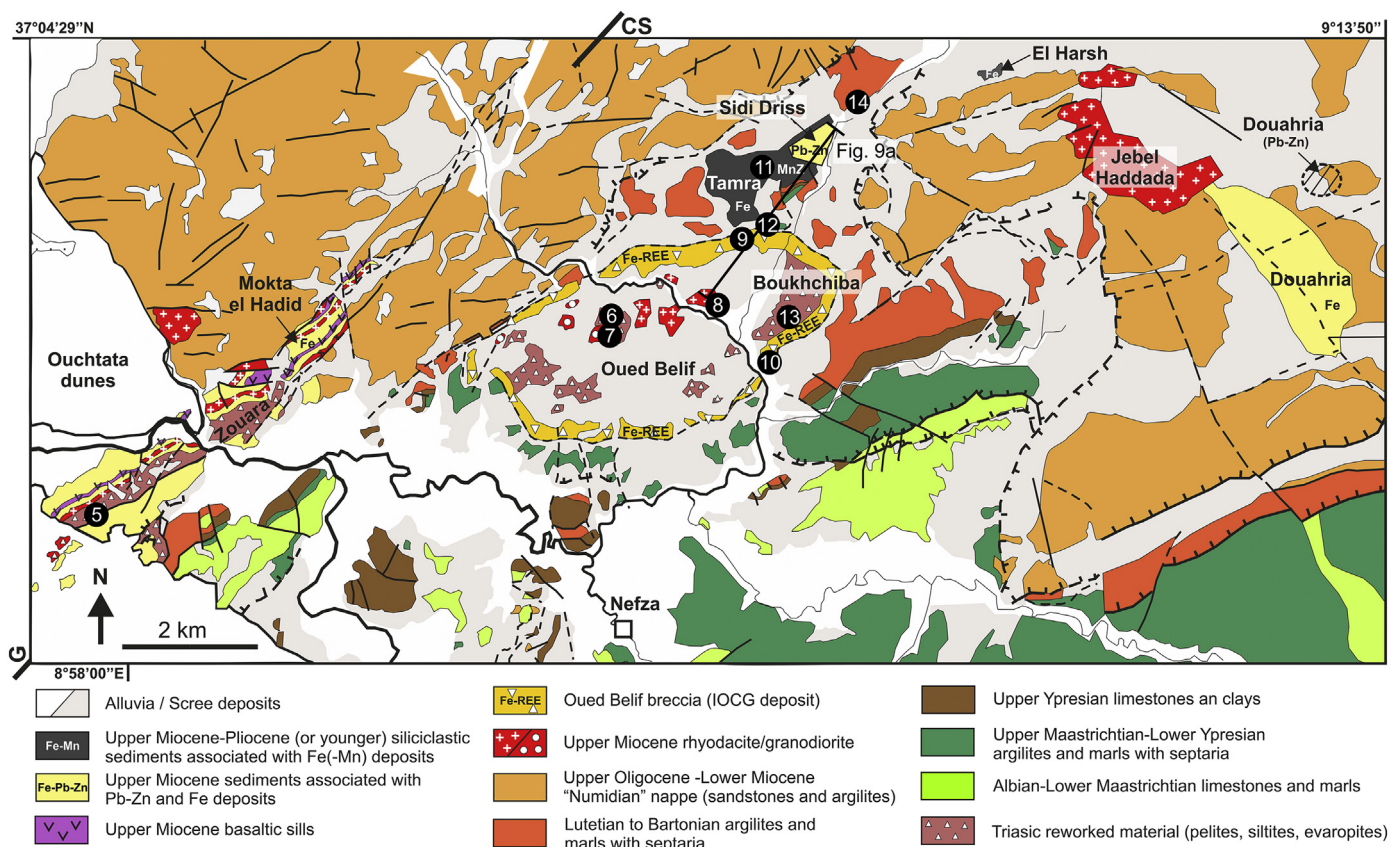
Fig. 2. Simplified geologic map of the Nefza district showing the location of the Tamra deposit in the northern part and the location of the cross section of Fig. 8a (modified after Gottis and Sainfeld, 1952; Batik, 1980; Rouvier, 1987). Numbers refer to sampling sites: 5-Ouchtata Triassic sediments (14OU03, OUCHTATA), 6-Chabet El Ain skarn (14CEA02), 7-Ragoubet El Alia granodiorite (OB48-79), 8-Ragoubet Sidi Ahmed rhyodacite (14AA02, OB45-42, OB45-78), 9-Tamra Oued Belif breccia (BR01), 10-Boukhchiba Oued Belif breccia (14OB02), 11-Tamra deposit (ABT1, CAT7, CAT7.5, ZMNWL8, 14TAM09, 14MnTAM, 14TAM07, CP04-3, CP04-35), 12-Tamra mine (south) marls (14TAM16), 13-Boukhchiba Fe-deposit (14BK01, 14BK11), 14-Tamra village marls (14ET02, 14ET03, EM04/11).

2013). This breccia encloses Triassic salt-related rocks linked to the top of a diapiric dome, and Serravalian-Late Tortonian magmatic bodies (Fig. 2). A regional shallow magmatic sill (20 km in diameter and up to 0.7–0.9 km in thickness) located 500 m below the Oued Belif structure is considered to be the root of magmatic activity in the Nefza area (Jallouli et al., 2003), and could be responsible for the high thermal gradient (> 100 °C/km) in the area (Jallouli et al., 1996). The origin of the IOCG Oued Belif breccia is likely to originate from mixing fluids between magmatic-hydrothermal, and basinal (evaporite) brines. K-Fe alteration event slightly predating the main mineralization is dated at 9.2 ± 0.25 Ma on adularia (Decrée et al., 2013). Subsequent magmatic activity during the Tortonian to Messinian (~8.4 and 6.9–6.4 Ma) erupted basaltic flows in the western part of the Nefza area (Fig. 2; Bellon, 1976; Rouvier, 1977, 1994) under extensional conditions (Mauduit, 1978; Maury et al., 2000; Jallouli et al., 2003).

Two generations of post-nappe continental to open-marine extensional basins overly the nappe pile and the magmatic rocks. They are both controlled by reactivation of NE-SW normal faults. The Sidi Driss and Douahria Messinian basins were inverted at the end of the Messinian period to form synclines (Fig. 2). They were composed of Late Miocene algal carbonates and/or evaporites (Decrée et al., 2008a), subsequently replaced by Pb-Zn sulphides, consisting of Messinian (or younger) SEDEX Pb-Zn deposit. The ore is characterized by galena and sphalerite, which is associated with As-bearing marcasite and pyrite, celestite, and barite. Mineralizing fluids have a maximum estimated temperature of 150 °C and are most likely influenced by Late Miocene magmatic activity (e.g., Messinian basalts, Decrée et al., 2008a). The Mio-Pliocene (or younger) Tamra basin unconformably overlies Eocene folded marls, the Oued Belif breccia (south) and the Sidi Driss basin

(east), (Fig. 2; Berthon, 1922; Dermech, 1990; Decrée et al., 2008b, 2010). The Tamra Formation is a siliciclastic sequence (Fig. 3) enriched in iron (Fig. 4a), which is interbedded with white clay lenses, the abundance of some of them having defined a specific "White Clay Zone" (Figs. 3 and 4b, c). In the area, two other ferruginous post-nappe basins are: 1) the Late Miocene Moktha el Hadid Formation, where hematite-rich halos surround basaltic flows, and 2) the Pliocene El Harch basin containing Tamra-like deposits (Decrée et al., 2008b, Fig. 2).

Middle to Late Miocene magmatic intrusions have enhanced hydrothermal fluid circulation that may be (at least partly) responsible for the numerous mineralizing events observed in the area (Decrée et al., 2013, 2014). Both magmatism and hydrothermal mineralization are related to a set of fractures inherited from the Variscan basement (Piqué et al., 2002). Miocene diapiric extrusions and late basaltic sills and dikes follow a NE-SW direction corresponding to the Ghardimaou-Cap Serrat sinistral shear zone (G-CS in Figs. 1 and 2). This major shear zone, thought to be of lithospheric scale (Decrée et al., 2016), directly or indirectly controlled several series of local mineral occurrences and deposits, such as the Oued Belif breccia and the Late Miocene Pb-Zn sedimentary exhalative (SEDEX) deposits of Sidi Driss and Douharia (Decrée et al., 2008a, 2013, 2014, 2016). In that context, the structural discontinuities (normal faults, thrust sheet boundaries, magmatic contacts and deformed plutons) are likely to have served as major fluid conduits (Fig. 4a; Decrée et al., 2008a). Other Cu-Ag-Au deposits are located along minor WSW-ENE fault zones in the area (Decrée et al., 2013, 2016). The Nefza area is still hydrothermally active, with numerous hot springs from 35 up to 70 °C (Gharbi, 1977; Zouiten, 1999) and regional thermal gradients up to 100 °C/km (Jallouli et al., 1996). Low discharge springs from 26 to 27 °C are present in the Sidi Driss
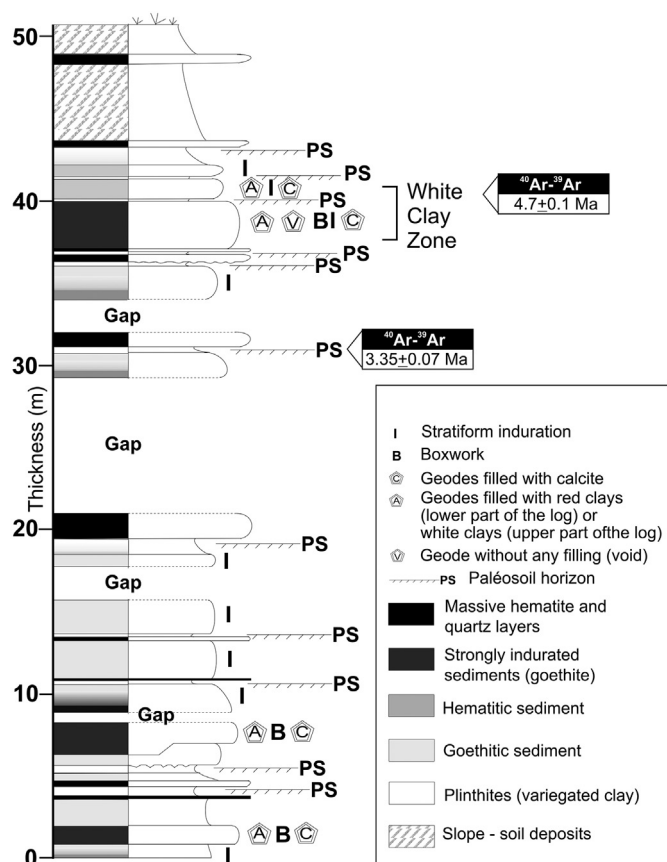
Fig. 3. Synthetic log of the Tamra Formation and location of the "White Clay Zone" (Decrée et al., 2008b). $^{40}Ar/^{39}Ar$ ages of hollandite group minerals are also indicated (Decrée et al., 2010).

(Stefanov and Ouchev, 1972; Dermech, 1990) and Tamra deposits (Decrée et al., 2010).

2.2. Tamra Fe-Mn deposit

The Fe-Mn Tamra mine is known since Roman times (Berthon, 1922) for its high content in iron (avg. 50 wt% Fe, Gottis and Sainfield, 1952). Since 1884, it has been intensively mined as some other parts of the Nefza mining district. Today, the low quality of the iron ore (~1% wt As) allows Tamra sediments to be used in the local cement industry. The eastern part of the deposit, which is overlying the Sidi Driss deposit, shows higher content of manganese oxides. It has been described as a distinct zone of the deposit (Fig. 2; Manganese Zone, MnZ; Decrée et al. 2008b).

The Tamra Formation is a 50-m thick siliciclastic and/or volcano-clastic series of ferruginous sediments, where almost all sedimentary textures have been overprinted by Fe(-Mn) oxide assemblages (Fig. 4a, Decrée et al., 2008b). Despite the lack of sedimentary structures, the whole Formation comprises an irregular succession of few centimeters to few meters thick shallowing-upward sequences, finishing by a sub-aerial/pedogenesis episode at the top of each sequence (Figs. 3 and 4a). Each sequence comprises: i) a basal 1-m thick highly indurated silici-clastic sedimentary unit composed of hematite and quartz, with an erosional base (*lower horizon*); ii) an intermediate fining-upward sequence of a few meters thick made up of reddish hematite-bearing sediments at the base, and yellowish goethite-bearing sediments at the top (*intermediate horizon*); and iii) an upper variegated mottled clay horizon, a few decimeters thick (*upper horizon*). Synsedimentary weathering/pedogenesis is thus well attested in the Tamra Formation.

The age of the Tamra Formation is not precisely known, but is supposedly Mio-Pliocene or younger according to the 1:50000 geo-logical map of Nefza (Rouvier, 1977, 1994) and the ^{40}Ar-^{39}Ar ages of 4.7 ± 0.1 Ma and 3.35 ± 0.07 Ma obtained on late Mn-oxides (Fig. 3, Decrée et al., 2010). These ages indicate a *per descensum* evolution of a weathering front from the upper part (older age) to the lower part (younger age), as well as a rapid deposition of the Tamra Formation during a regional extensional tectonic regime (Fig. 4a, Bouaziz et al., 2002). Bouzouada (1992) describes this basin as a synclinal structure with E-W to ENE-WSW axis to the west, and NNE-SSW to the east. A fault network of directions N-S to N140, N10 to N40 and E-W has affected this basin and has played an important role in the variation of facies both vertically and laterally. The normal faults N-S, N140 and E-W are indeed synsedimentary faults (Fig. 4a).

The primary early diagenetic and/or pedogenetic pre-concentration of iron is linked to meteoric fluids feeding temporary aquifers, which were involved in seasonal Fe concentration processes (Fig. 5; *Stage 1*; Decrée et al., 2008b). Primary pedogenesis was reinforced by a re-current progressive and pervasive polycyclic pedogenesis of each se-dimentary sequence (Decrée et al., 2008b). It corresponds to the main pedogenic Fe event that has provided the current iron ore in the Tamra deposit (Fig. 5; *Stage 2*). A primary Fe-rich sedimentary deposition could also be considered given the nearby Oued Belif breccia (Decrée et al., 2008b). Decrée et al. (2010) have proposed a refined analyzes of the Mn mineralization and the effect of hydrothermal fluids on the chemistry of the ore after the primary pedogenic/diagenetic enrich-ment. According to them, this hydrothermal enrichment was super-imposed on the weathering conditions found in the Tamra sequence at the same time, and has led to the formation of Mn-oxides, first with hollandite, romanechite and Sr-cryptomelane at 4.7 ± 0.1 Ma (Fig. 5; *Stage 3*), and then coronadite, chalcophanite, amorphous Mn-oxides and kaolinite at 3.35 ± 0.07 Ma (Fig. 5; *Stage 4*). Mn—oxides ex-tensively occur as coatings filling fractures, creating *per descensum* structures commonly found in other supergene manganese deposits of North Africa (Dekoninck et al., 2016a, b; Verhaert et al., 2018). The hydrothermal contribution is supported by enrichment in Fe, Mn, Pb, Zn and As in the later stages (Fig. 5; *Stages 3 and 4*), and is considered to be the result of fluid-driven hydrothermal circulation in the underlying Sidi Driss Pb-Zn deposit, which is enriched in those elements (Decrée et al., 2008a, b, 2010). Such hydrothermal activity is also supported by (i) the high regional thermal activity, (ii) the high geothermal gradient (Jallouli et al., 2003), (iii) the emplacement of late sulphide deposits (Fig. 4d; Decrée et al., 2008b, 2016), and (iv) the occurrence of thermal springs throughout the district (e.g., Decrée et al., 2010). Intense local fracturing has allowed for the circulation of hydrothermal and meteoric fluids, which have promoted the alteration of sand and the formation of clays (Fig. 4a). Messinian magmatism could have influenced the cir-culation of mineralizing fluids at least during the earlier stages of the ore formation. The occurrence of late and reduced mineral veins (ga-lena, pyrite and siderite) crosscutting the whole Tamra Formation contrasts with the highly oxidized minerals of the Tamra deposit (Fig. 4d). These veins probably reached temperatures close to 80 °C in the Sidi Driss sulphide deposit, as noted by Decrée et al. (2008a), and 30 °C in several recent springs of the Nefza district (Stefanov and Ouchev, 1972; Gharbi, 1977; Zouiten, 1999; Dermech, 1990). Three acidic springs occur in the Tamra mine (5–6 pH units, Decrée et al., 2010).

2.3. Kaolinite-halloysite formation

White clay assemblages composed of kaolinite and halloysite have been observed in several spots in the Tamra deposit, but mainly in the "White Clay Zone" with relatively low lateral extension (Figs. 3 and 4b, c). Kaolinite-halloysite usually fills open cavities or porosity, and re-places primary 2:1 smectites (Decrée et al., 2008b). Their formation is considered to be the result of early pedogenetic/weathering processes affecting each sequence, as well as the downward percolation of
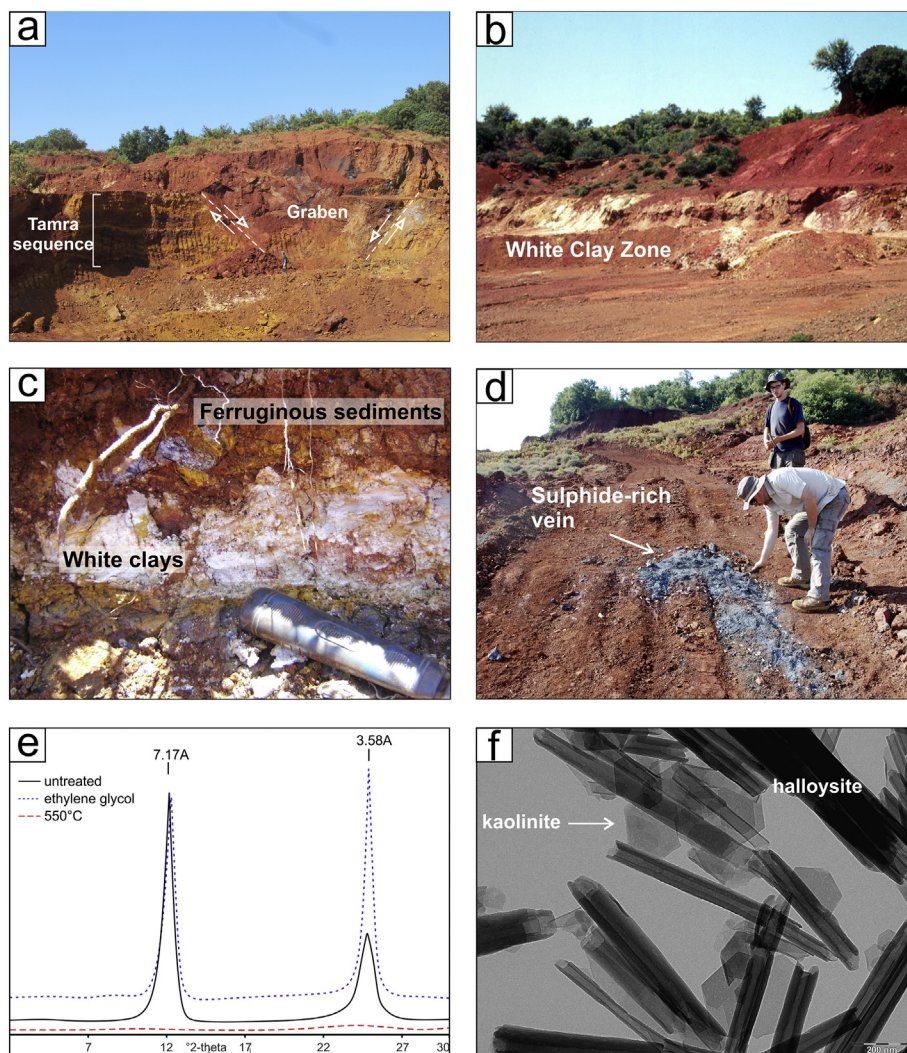
Fig. 4. a) Overview of the ferruginous Tamra sequence affected by normal faults. b) Iron mine of Tamra showing the "White Clay Zone" in the ferruginous sediments. c) Focus on a white clay level embedded in the ferruginous matrix. d) Late sulphide-rich vein (pyrite, galena and siderite) crosscutting the whole Tamra Formation. e) XRD pattern of Tamra white clays (sample 14TAM09) showing the typical 7.17A reflectionand 3.59A harmonic. f) TEM view of typical halloysite nanotubes and hexagonal flakes of kaolinite in sample HT1 (Decrée et al., 2008b; Moussi, 2012).
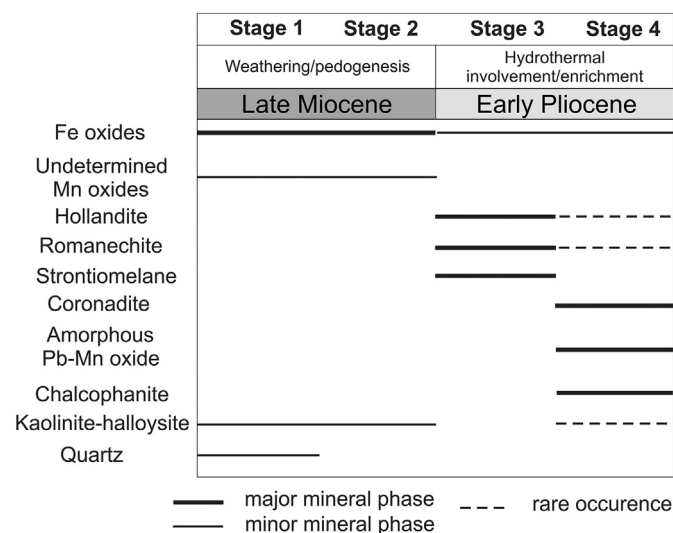

Fig. 5. Paragenetic sequence of the mineral phases showing the 4 stages observed in the Tamra Fe-Mn deposit (modified after Decrée et al., 2010).

meteoric fluids during late weathering/diagenetic stages, the latter being observed only in the upper part of the Tamra sequence (Decrée et al., 2008b). Most of the kaolinite-halloysite levels are associated with early mineralization stages (Fig. 5; *Stages 1 and 2*). However, minor amounts of these minerals could be intimately mixed with late stage Mn-oxides (Fig. 5; *Stage 4*) suggesting that they are connected to hydrothermal inputs (Decrée et al., 2010).

White clays are present in the *intermediate horizon* defined by Decrée et al. (2008b), where they form micro-aggregates in association with Fe (III) minerals. The horizon is indurated by hematitic sediments at the base and goethitic sediments at the top, which are responsible for geodic cavities filled by kaolinite and halloysite. This *intermediate horizon* undergoes a nearly complete weathering/alteration, which has led to a heavy remobilization of iron and the formation of goethite and hematite, as well as the neoformation of 1:1 white clays by recombination of released Si and Al. The occurrence of white clay spots in the mottled gray clay *upper horizon* (only a few centimeters thick) would be linked to the transformation of primary 2:1 smectites in cation-free 1:1 clays than to their neoformation in cavities as it was observed in the *intermediate horizon* (Decrée et al., 2008b). A late diagenetic evolution phase has turned the upper 20 m of the Tamra Formation into pure Fe-free white 1:1 clays, coevally to the

Table 1

Stable isotope composition of the Nefza area rocks. *: replicate analyzes, +: decarbonated sample, WR: whole rock sample, < 2 μm: oriented aggregates with < 2 μm fraction preparation, Q: quartz, Kaol: kaolinite, I: illite, Gt: goethite, Hem: hematite, Py: pyrite, H: halloysite, Cal: calcite, Fsp: feldspars, Sm: smectite, Chl: chlorite, I-Sm: intermixed layers of illite-smectite, Pl: plagioclase, Kfs: K-feldspar, Mcs: micas, Gs: gypsum, Am: amphibole. ONM sample comes from drill cores of the "Office National des Mines". See Figs. 1 and 2 for the location of the sample (column 3).

Label	Material type	Outcrop label	Age	Mineralogy	$\delta^{18}O_{VSMOW}$ (‰)	δD_{VSMOW} (‰)	H_2O wt%	$\delta^{18}O_{carb\ VSMOW}$ (‰)	$\Delta^{13}C_{carb\ VPDB}$ (‰)	Material origin
ABT1 (< 2 μm)	White clay	Tamra mine (11)	Late Miocene - Pliocene	Kaol, H	19.2	−91	9.8			Moussi (2012)
14TAM09 (< 2 μm)					21.9	−72	14.9			This issue
CAT7,5 (< 2 μm)					21.3	−93	9.7			Moussi (2012)
CAT7 (< 2 μm)					23.8	−123	16.4			
ZMNWL8 (< 2 μm)*					24.3	−95	10.3			
					25.4	−70	17.2			
14MnTAM (WR)	Fe ore			Gt	−2.0	−127	12.7			This issue
CP04-3 (WR)				Hem, I, I-Sm, Q	−1.0	−156	7.4			Decrée et al. (2008b)
CP04-35 (WR)				Gt, Hem, I, I-Sm, Q	5.1	−142	3.2			
14TAM07 (WR)				Gt, Hem	−1.3	−132	6.0			This issue
14OU03 (WR)		Ouchtata (5)	Trias	Gt, Py, Q	N.A.	−132	5.4			
OUCHTATA (WR)				Gt, Hem	0.2	−125	8.5			
OMS2 (WR)	Claystone	Om-Tebal (4)	Oligocene (Numidian)	Q, Kaol, I	18.8	−72	8.4			Moussi (2012)
14SB02 (< 2 μm)		Sidi Bader (2)		Q, Kaol, I	16.1	−63	8.9			This issue
14 AD01 (< 2 μm)*	Sandstone	Ain Drahan (1)		Q, Sm, Kaol	18.0	−59	11.0			
					18.4					
14SB01 (WR)*		Sidi Bader (2)		Q, Kaol	14.5	−75	1.4			
					14.6					
14TAM16 (< 2 μm)	Marl	Tamra mine (12)	Lutetian-Bartonian		23.5	−61	14.8	26.6	1.10	
14ET03 (WR)	Marl (septaria)	Tamra village (14)		Cal, Q, Fsp	–	−96	–	28.8	−0.12	
14ET02 (WR)	Marl (weathered)			Cal, Q, Kaol	–		11.9	27.4	−1.30	
14ET02+				Q, Kaol	–	−72	–	–	–	
EM04/11 (WR)		Ain Sebaa (3)	Albian-Maastrichtian	Q, Cal, Kaol, Sm	–	−64	7.7	23.8	−0.21	ONM
14ME02 (< 2 μm)				Q, I	25.8	−65	4.5	25.6	−0.78	This issue
OB48-79 (WR)	Skarn	Ragoubet El Alia (7)	Serravalian-Tortonian	Cal, Gp, Am, Q	27.4	−67	3.2	28.2	1.23	Ben Abdallah (2013)
14CEA02 (WR)	Skarn (weathered)	Chabet El Ain (6)		Cal, Q, Fsp	–	−92	0.5	27.6	1.05	This issue
14OB02 (WR)	Oued Belif breccia	Boukhchiba (10)	< Tortonian	Gt, Kfs, Q	3.9	−132	9.4			
14BK11 (WR)		Boukhchiba (13)		Gt, Kfs	−1.6	−132	12.4			
BR01 (WR)		Tamra mine (9)		Gt, Kfs, Q	5.9	−113	8.3			
14AA02 (< 2 μm)	Rhyodacite ((weatherered) (weathered))	Ragoubet Sidi Ahmed (8)		Sm, Kaol	20.7	−68	9.1			
14BK01 (WR)	Rhyodacite	Boukhchiba (13)		Q, I, Kaol, Sm, Chl	15.9	−72	5.6			
14BK01 (< 2 μm)*					18.8	−48	13.3			
					19.3	−48				
OB45-78 (WR)	Granodiorite	Ragoubet Sidi Ahmed (8)	Serravalian-Tortonian	Pl, Kfs, Q, Mcs	15.1	−84	0.4			Ben Abdallah (2013)
OB45-42 (WR)	Granodiorite (weathered)		< Tortonian	Kfs, Pl, Q, Mcs	16.0	−80	0.7			

Table 2

Chemical composition of the white clays CAT7, CAT7.5, ABT1 and ZMNWL8 determined by X-ray fluorescence, using a Panalytical Axios Dispersive XRF Spectrometer. The loss-on-ignition was evaluated from the weight difference between samples heated at 100 °C and 1000 °C. - = not analyzed. The results are expressed in weight concentration percent of oxides (Moussi et al., 2011; Moussi, 2012).

	SiO_2	Al_2O_3	Fe_2O_3	MgO	MnO	CaO	Na_2O	K_2O	P_2O_5	TiO_2	H_2O	Total
CAT7	41.37	36.14	4.56	0.08	< 0.01	0.04	0.07	0.07	< 0.01	0.06	17.6	100
CAT7,5	43.53	39.15	0.24	0.04	0.01	0.05	0.03	< 0.02	0.03	0.01	16.9	100
ZMNWL8	43.64	39.16	0.53	–	–	0.1	–	0.42	0.04	0.03	14.2	98.12
ABT1	39.38	36.55	0.52	–	–	0.1	–	0.03	0.03	0.02	22.9	99.53

neoformation of Mn-oxides. The reconcentration and/or precipitation of pure Fe-free white clays at the interface between lithologies with contrasting permeability is linked to the destabilization of clay aggregates in the upper part of the profile, to their migration, and finally to their precipitation in cavities at the interface with impervious layers. According to this process, halloysite could be locally dominant (Fig. 4b, c; Decrée et al., 2008b). Some similarities with the Boukhchiba and Douahria mines (location in Fig. 2) can be found taking into account the occurrence in both deposits of white clay levels and nodules.

3. Materials and methods

3.1. Mineralogical analyzes

Mineralogical analyzes of bulk rock samples (14MnTAM, 14TAM07, 14OU03, OUCHTATA, 14SB01, 14ET02, 14ET03, EM04/11, OB48-79, 14CEA02, 14OB02, 14BK11, BR01, 14AA02, 14BK01, OB45-78, OB45-42) and oriented aggregates (14TAM09, 14SB02, 14 AD01, 14TAM16, 14ME02, 14AA02, 14BK01) have included X-ray diffraction (XRD) at the PC2 platform (UNamur) using an X-ray Panalytical X'Pert Pro and a PHILLIPS diffractometers (CuKα radiation; Table 1). Oriented aggregates were treated with ethylene glycol and heated at 550 °C, following the methodology of Holtzapffel (1985; Fig. 4e). Other mineralogical analyzes from Moussi (2012; ABT1, CAT7.5, CAT7, ZMNWL8, OMS2) and Decrée et al. (2008b; CP04-3, CP04-35) have been taken into account. Clay samples were further investigated at the University of Namur (Belgium), using a transmission electron microscope Jeol JEM 100 CX II, with an emission source of 100 kV. Samples must be transparent to electrons. Hence, depending on their nature, their thickness had to be < 30–100 nm, a condition which was generally met with diluted suspensions of natural clays. A drop of the suspension is air dried on a Cu grid, coated with a thin carbon film in which microscopic holes were drilled.

3.2. Stable isotope geochemistry

A total of twenty-nine samples were analyzed: eighteen were samples collected in the field (14TAM07, 14TAM09, 14MnTAM, 14TAM16, 14OU03, OUCHTATA, 14SB01, 14SB02, 14 AD01, 14ET02, 14ET03, 14ME02, 14CEA02, 14OB02, 14BK01, 14BK11, BR01, 14AA02), and eleven were previously collected by Decrée et al. (2008b; CP04–3, CP04–35), Moussi (2012; ABT1, CAT7.5, CAT7, ZMNWL8, OMS2), Ben Abdallah (2013; OB45-78, OB45-42, OB45-79) and the "Office National des Mines de Tunisie" (ONM; EM04/11; Table 1; Figs. 1 and 2). The twenty-nine samples were analyzed at the Institute of Earth Surface Dynamics of the University of Lausanne (Switzerland) for their oxygen and hydrogen isotope compositions. Silicates (quartz, feldspars, clays; Table 1) and oxides (goethite-hematite) were analyzed for their $\delta^{18}O$ values in all rock types (rhyodacites, claystones, sandstones, marls, skarns). Hydrogen isotope compositions were measured on hydrous silicates (kaolinite-halloysite), and hydroxides (goethite-hematite; Table 1). Five samples of the white clay levels (outcrop 11 in Fig. 2; ABT1, 14TAM09, CAT7.5, CAT7, ZMNWL8) and four of Fe(III) minerals (outcrop 11 in Fig. 2; 14MNTAM, CP04-3, CP04-35, 14TAM07) were collected respectively in the kaolinite-halloysite levels and goethite-

hematite concretions in the Tamra deposit. In order to compare the conditions of the Tamra ores with other places in the Nefza district, two samples with high goethite-hematite content from Triassic weathered pyrites (outcrop 5 in Fig. 2; 14OU03, OUCHTATA), which were contained in carbonates, were added to the Fe-oxide set, as well as three samples of the ferruginous deposits from Oued Belif (outcrops 9, 10 and 13 in Fig. 2; 14OB02, 14BK11, BR01) In addition, other samples were collected from the bedrock of the Nefza area to analyze the stable isotopic composition of oxygen and hydrogen. Finally, other samples were analyzed for their H and O stable isotope compositions (Table 2): samples of two granodiorites in borehole OB45 at Ragoubet Sidi Ahmed (outcrop 8 in Fig. 2; OB45-78, OB45-42), two rhyodacites at Boukhchiba (outcrop 13 in Fig. 2; 14BK01) and Ragoubet Sidi Ahmed (outcrop 8 in Fig. 2; 14AA02), two skarns at Chabet El Ain (outcrop 6 in Fig. 2) and Ragoubet El Alia (outcrop 7 in Fig. 2, 14CEA02), 5 marls at Tamra mine (outcrop 12 in Fig. 2; 14TAM16), Tamra village (outcrop 14 in Fig. 2; 14ET02, 14ET03, EM04/11) and Ain Sebaa (outcrop 3 in Fig. 1; 14ME02), two clayey levels at Om-Tebal (outcrop 4 in Fig. 1; OMS2) and Sidi Bader (outcrop 2 in Fig. 1; 14SB02) and two sandstones of the Oligocene Numidian sandstone at Ain Drahan (outcrop 1 in Fig. 1; 14 AD01) and Sidi Bader (outcrop 2 in Fig. 1; 14SB01).

All silicates and Fe-hydroxides of the Nefza area were analyzed for their oxygen isotope compositions. These analyzes were obtained using a CO_2-laser fluorination line coupled to a Finnigan MAT 253 gas source mass spectrometer according to a method, which was adapted after Vennemann et al. (2001). Between 2 and 3 mg of non-carbonated powder were loaded onto a small Pt-sample holder and pumped out to a vacuum of about 10^{-6} mbar. After prefluorination of the sample chamber, the samples were heated with a CO_2-laser in the presence of pure F_2. Excess F_2 was separated from the O_2 produced by conversion to Cl_2 by KCl held at 150 °C. The extracted O_2 was then introduced into the inlet of the mass spectrometer. Oxygen isotope compositions are given in the standard δ-notation and are expressed relative to the Vienna Standard Mean Ocean Water (VSMOW) in permil (‰). Replicate oxygen isotope analyzes of the LS-1 in-house quartz standard gave an average value of 18.10 ± 0.06‰ (2SD, $n = 4$) for $\delta^{18}O$. The oxygen and carbon isotope compositions of carbonates (marls, skarns) were determined on 100 to 1200 μg whole rock or carbonate powders using 100% H_3PO_4 dissolution at 70 °C with an automated GasBench II preparation unit attached to a Thermo Finnigan DeltaPlus XL mass spectrometer and a He-carrier gas system (Spötl and Vennemann, 2003). The results are given in the standard δ-notation, which is expressed relative to VSMOW in permil (‰) for oxygen and relative to VPDB for carbon. Reproducibility for the analyzes estimated on the basis of repeated analyzes of the in-house Carrara Marble standard (CM; $n = 9$), gave an external precision (1SD) of ± 0.11‰ for $\delta^{18}O$ and 0.08‰ for $\delta^{13}C$.

The hydrogen isotope composition of clay, Fe-oxides and bulk samples together with their water content were determined with a zero-blank auto-sampler and a High-Temperature Conversion Elemental Analyzer (TC-EA; Bauer and Vennemann, 2014) after drying in a vacuum desiccator overnight. The amount of powder needed for Fe-oxides is between 2 and 3 mg, 0.5–1.0 mg for kaolinite samples, 3.0–4.0 mg for clayey samples and 4.0–5.0 mg for whole rock materials. Marls were decarbonated before the measurements. In-house reference materials of

Table 3
Lead isotope ratio of kaolinite-halloysite samples of the Tamra deposit. 2se refers to 2 standard errors, *: replicate analyzes.

Sample	Age	$^{208}Pb/^{204}Pb$	2se	$^{207}Pb/^{204}Pb$	2se	$^{206}Pb/^{204}Pb$	2se
14TAM09 (< 2 μm)	< Zanclean	38.8671	0.0026	15.6681	0.0009	18.7720	0.0010
ABT1		38.8403	0.0022	15.6629	0.0009	18.7716	0.0010
CAT7		38.8446	0.0015	15.6699	0.0006	18.7611	0.0006
CAT7,5*		38.8654	0.0016	15.6687	0.0006	18.7786	0.0007
		38.8592	0.0014	15.6679	0.0006	18.7785	0.0006
ZMNWL8		38.8623	0.0015	15.6670	0.0006	18.7763	0.0007

biotite (G1; δD = −64 ± 1.6‰) and kaolinite (K-17; δD = −125 ± 1.3‰) were used to calibrate the measured isotopic compositions (Bauer and Vennemann, 2014). The isotopic composition of hydrogen is expressed in the "δ-notation", relative to VSMOW in permil (‰). All the measurements of samples and standards were replicated but only their average value are presented in Table 1.

3.3. Pb-Pb isotope measurements

Pb isotopic analyzes were performed on five kaolinite-halloysite samples (Table 3) at the Laboratoire G-Time (Université Libre de Bruxelles, ULB, Belgium). The total acid dissolution and lead purification were realized according to the procedure described in Weis et al. (2006) and Renson et al. (2011). The Pb isotopes were measured on a Nu Plasma Multi-Collector Inductively Coupled Plasma Mass Spectrometer (MC-ICP-MS from Nu Instruments) by applying a static multi-collection in dry mode. Tl standard solution was added as dopant to all samples and Pb standards (Pb-Tl ratio of 4 or 5) in order to automatically correct the Pb isotopic ratios for mass fractionation bias. Also, the sample standard bracketing method was applied to correct instrumental drift. During the period of analyzes, repeated measurements of the Pb NBS981 standard (n = 22) gave average values of $^{208}Pb/^{204}Pb$ (± 2σ$_n$; 36.7134 ± 0.0008), $^{207}Pb/^{204}Pb$ (15.4968 ± 0.0003) and $^{206}Pb/^{204}Pb$ (16.9406 ± 0.0004). All the reported values were normalized using the recommended values from Galer and Abouchami (1998): $^{208}Pb/^{204}Pb$ (36.7219 ± 0.0044), $^{207}Pb/^{204}Pb$ (15.4963 ± 0.0016) and $^{206}Pb/^{204}Pb$ (16.9405 ± 0.0051).

4. Mineralogy

Whole rock samples of ABT1, CAT7, CAT7.5, ZMNWL8 (Moussi, 2012) and 14TAM09 had a composition of 100% of phyllosilicates. However, some variations in the SiO_2 content of the chemical composition of ABT1, CAT7, ZMNWL8 and CAT7.5 might indicate the presence of quartz (Table 2; Moussi et al., 2011; Moussi, 2012). When heated by laser ablation in the oxygen isotope protocol, these samples show a small amount of quartz grains. The increase in the Fe_2O_3 content, especially in sample CAT7, and the occurrence of pinkish/reddish tints in the white clays might be due to disseminated co-genetic Fe-oxides (Fig. 4c; Table 2). The fraction < 2 μm (Brindley and Brown, 1980) consists of kaolinite (Fig. 4e, Table 1), while halloysite is evidenced by TEM images, which shows the typical tube structure in association with hexagonal flakes of kaolinite (Fig. 4f, Caillère et al., 1982).

5. Stable isotope results

All new following results focus on the Tamra ores, first presenting the kaolinite-halloysite white clays (Fig. 6a), and then the associated Fe-oxides δ18O and δD values (Fig. 6b). These items are finally integrated in the large set of δ18O and δD values of the country rock types (Fig. 6c; magmatic, metamorphic and sedimentary), in order to have a better view of these stable isotopes in the Nefza area. In addition, new Pb-Pb isotopes of the kaolinite-halloysite are considered in the set of data already studied by Decrée et al. (2013, 2014; Fig. 7).

5.1. δ18O—δD values

The kaolinite-halloysite samples are strongly enriched in 18O, with δ18O values from 19.2 to 25.4‰, while δD values are between −70 and −123‰ (Fig. 6a; Table 1). The effect of detrital quartz on the isotopic composition would be a decrease in the δ18O values, considering that quartz from high temperature rocks (magmatic and metamorphic rocks) and of non-diagenetic origin would generally have lower $^{18}O/^{16}O$ ratios compared to clay minerals formed at low temperatures (e.g., Savin and Epstein, 1970). In the diagram (Fig. 6a), all kaolinite-halloysite samples plot on the right side of the "kaolinite line" defined by Savin and Epstein (1970), which is considered to be the normal trend for kaolinite in equilibrium with meteoric waters at 25 °C.

In the Tamra deposit, goethite and hematite are often associated with small amounts of quartz and clays (Decrée et al., 2008b). Despite that the absolute δ18O and δD values differ from those of the kaolinite-halloysite, they both have similar trends. Two samples plot along the 25 °C line of Yapp (1990), which is considered as an equivalent of the kaolinite line for goethite (δ18O = −1.3 and −2.0‰, δD = −127 and −132‰), while two other samples are close to the temperature lines that would correspond to fractionations established at 0 °C (δ18O = −1.0 and 5.1, and δD = −142 and −156‰; Fig. 6b). Some of the goethite-hematite were clearly in equilibrium with meteoric waters, as they plot on the 25 °C line. However, some of them could be in disequilibrium with temperatures below 25 °C (Fig. 6b), as already shown in kaolinite-halloysite samples. These goethite and hematite could also have been contaminated by small amounts of quartz and clay impurities (Table 1). The comparison of Tamra iron ores with other Fe-oxides in the district shows that Ouchtata goethite, which are hosted in Triassic carbonates, plots along the 25 °C line (Fig. 6b) and obviously results from the weathering of Triassic pyrite. However, some Fe-oxides of the Oued Belif breccia have higher δ18O values compared to the Ouchtata weathering Fe-oxides, which may be explained by a small quantity of quartz and K-feldspars in the ferruginous matrix (Decrée et al., 2013), or even by the influence of hydrothermal fluids that could have precipitated the Fe-oxides (Fig. 6b and c; Table 1).

Plutonic and volcanic rocks in the Nefza area have high δ18O values for igneous rocks of granitic composition (15.1 to 16.0‰) and δD (−72 to −84‰), when compared to values compiled by Hoefs (2009). This might suggest some late low-temperature alterations of these rocks. Alternatively, they might include a higher contribution of the S-type granites (e.g., Hoefs, 2009), as suggested by the peraluminous trend of some rhyodacites (Decrée et al., 2014). The clay fraction of their weathering products has higher δ18O and δD values, with a range between 19.0 and 20.7‰, and − 48 and − 68‰ respectively (Fig. 6c). These values differ from the Tamra white clays δ18O and δD, probably because the mineral assemblage is composed of smectite, kaolinite, illite and chlorite (Table 1).

The metamorphic rocks in the close vicinity of the Tamra deposit are represented by scarce skarns, when in contact with plutonic rocks and Cretaceous to Eocene marls (Fig. 2, Decrée et al., 2013). The δ18O values of these skarns are the highest of the area, probably because the primary carbonates were deposited in a marine environment. From bulk rocks, the separated carbonate fractions have δ18O values between 27.6 and 28.2‰, while the δD values of the hydrous silicate fraction vary
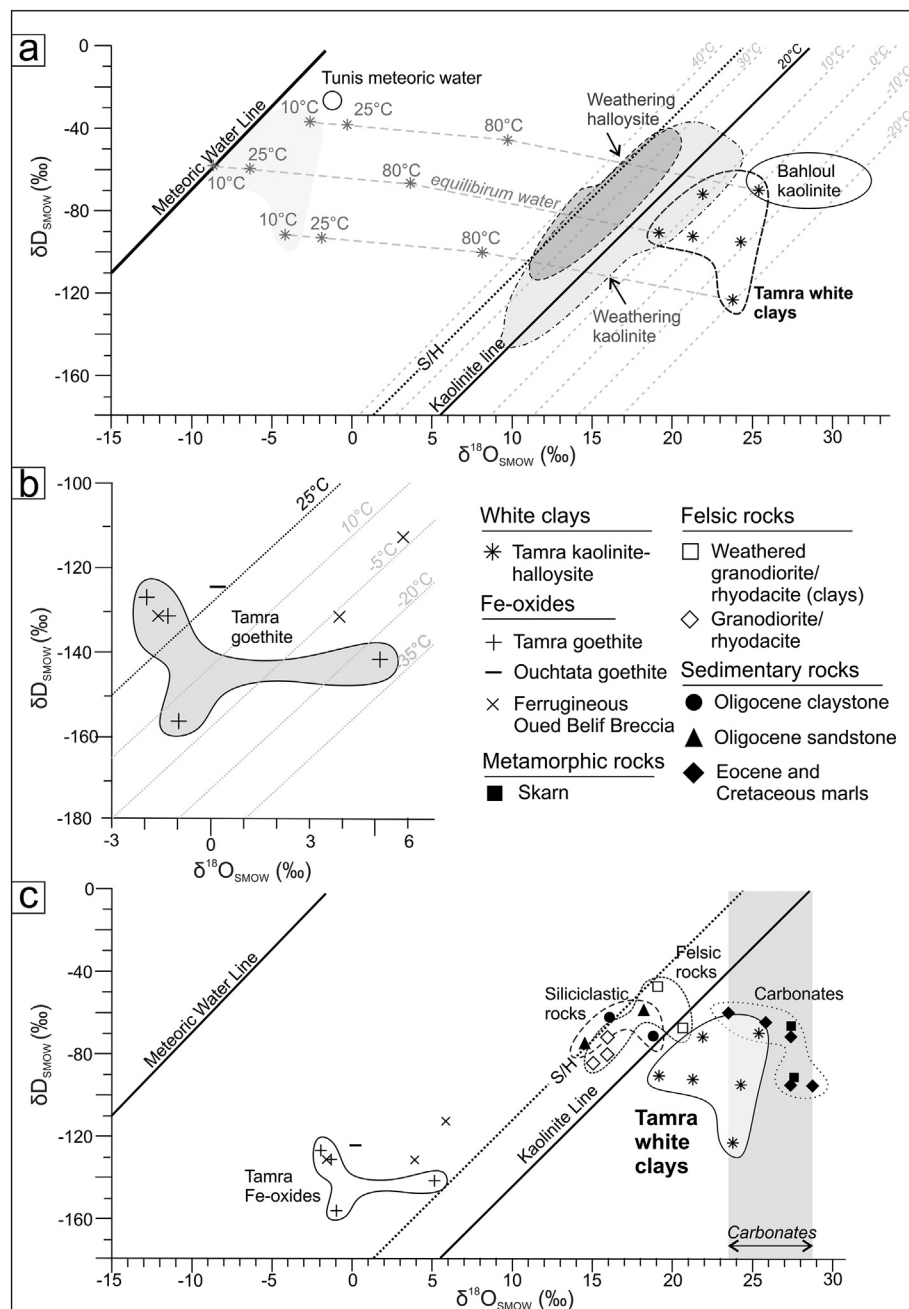
Fig. 6. a) δD and δ^{18}O plot of kaolinite-halloysite samples of the Tamra Formation, with known data of weathering kaolinite (gray area) and halloysite (dark gray area, Sheppard and Gilg, 1996) as well as kaolinite of the Bahloul Formation hosting the Bou Grine Pb-Zn deposit (Bechtel et al., 1999). Calculated equilibrium waters at 10 °C, 25 °C and 80 °C are represented by light gray stars connected by dashed lines. The meteoric water, kaolinite weathering (Savin and Epstein, 1970) and supergene/hypogene lines (S/H, Sheppard and Gilg, 1996) are given for reference. Intermediate temperature lines are calculated from equations in Sheppard and Gilg (1996). b) Goethite and hematite samples of the Nefza area in a δD and δ^{18}O plot. Temperature lines are calculated from Yapp (1990). c) δD and δ^{18}O plot showing the stable isotope compositions of felsic, siliciclastic and carbonate rocks with Fe-oxides and white clays of the Tamra mine (Table 1). Carbonate values are indicated in gray shades on the right of the diagram. Carbonate range of values are given by gray shades.

from −67 to −92‰ (Fig. 6c; Table 1). Therefore, only clay minerals contain hydrogen in their structure and provide enough hydrogen to be properly analyzed for their δD values.

The Cretaceous to Eocene marls show values enriched in ^{18}O, reaching 28.8‰, which are similar to the δ^{18}O values of the skarn (Fig. 6c, Table 1). In detail, the O isotope compositions in calcite from marls (23.8 to 28.8‰; gray shade area in Fig. 6c) are enriched in ^{18}O in contrast to the clay (and quartz) fraction within these same host rocks (kaolinite, illite, and quartz; 22.3 to 25.8‰). The δD is only analyzed in the clay fraction within these rocks, ranging from −64 to −96‰, due to only clay minerals that could contain hydrogen in their structure.

The δ^{18}O of the Oligocene sandstones range from +14.5 to +18.4‰, and their δD from −59 to −75‰ (Fig. 6c). These isotopic compositions reflect the abundance of quartz and subordinate amounts of kaolinite and smectite. The δ^{18}O and δD values from the Numidian claystone lenses interlayered with the sandstones are similar (δ^{18}O = 16.1 and 18.8‰, δD = −63 and −72‰). All data obtained

from the Oligocene whole rocks plot on the left side of the kaolinite line (Fig. 6c).

5.2. Pb-Pb isotope composition

The Pb isotopic ratios of the white clay samples from the Tamra formation have been integrated in the large set of Pb isotope data available for the Nefza district (Fig. 7; Decrée et al., 2014). No age correction on the Pb isotopic ratios were needed, given their relatively recent age of formation (Late Miocene). Kaolinite-halloysite samples show similar ^{206}Pb/^{204}Pb (18.761–18.779) and ^{208}Pb/^{204}Pb (38.840–38.867) ratios, falling in a narrow window (Fig. 7, Table 3). As a whole, the Pb isotopic data of the white clays belong to a trend defined by the Pb-Pb values from various mineral occurrences of the district, including the Oued Belif breccia ferruginous matrix (Decrée et al., 2013), the Tamra, Douharia, El Harsh, Mokta el-Hadid Fe-oxides, and the Sidi Driss and Douharia galena (Fig. 7; Decrée et al., 2014).
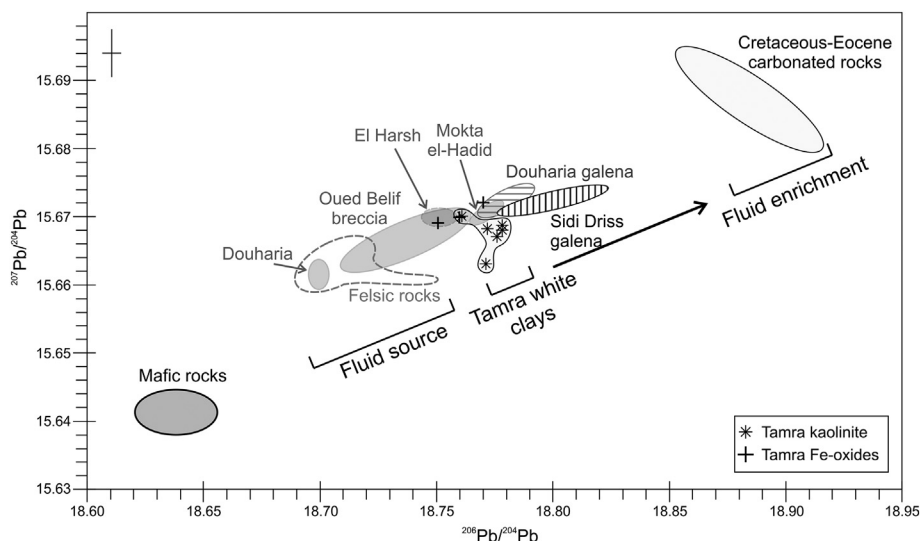
Fig. 7. Fe-oxides of Douharia, Oued Belif breccia, El Harsh, Mokta el-Hadid, and galena of the Douharia and Sidi Driss deposits (modified after Decrée et al., 2014) together with the Tamra white clay levels plotted on a $^{207}Pb/^{204}Pb$ vs. $^{206}Pb/^{204}Pb$ diagram (Table 3). Felsic rocks and Cretaceous-Eocene carbonated substratum rocks are also reported on this graph (Decrée et al., 2008a, b). Pb isotopic ratios are not recalculated for the white clays of Tamra considering recent age of the samples. The error bar represents the mean for the standard deviations.

6. Origin of the white clays in the Tamra ores

The unusual stable isotope compositions recorded in the halloysite-kaolinite of the Tamra deposit are not in equilibrium with pure meteoric waters: the combined $\delta^{18}O$ and δD values of pure kaolinite-halloysite plot on the right side of the kaolinite reference line. The $\delta^{18}O$ values are higher than those of detrital kaolinites (Fig. 6a; Sheppard and Gilg, 1996) and also higher temperature kaolinite (hydrothermal). The measured stable isotope compositions correspond to unrealistic temperature conditions below 0 °C (Fig. 6a). For instance, the calculated isotopic compositions of the coexisting water, which are in equilibrium with the kaolinite and halloysite at 10 to 25 °C, show higher $\delta^{18}O$ values compared to the meteoric water line that represents the present day meteoric water for kaolinite formed at 25 °C. The isotope composition of weathering halloysite as compiled by Sheppard and Gilg (1996), plots on the left side of the kaolinite line (light gray area in Fig. 6a). Mixing those regular halloysite crystals with kaolinite would produce a decrease in $\delta^{18}O$, which is not recorded in the Tamra white clays. Furthermore, co-genetic Fe-oxides show the same trend compared to white clays, i.e. high $\delta^{18}O$ values for some goethites are reported on the right side of the 25 °C line (for goethite after Yapp, 1990), which strengthens the interpretation based on the values of $\delta^{18}O$ and δD (Fig. 6b). Nevertheless, some of these goethite and hematite crystals plot on the equilibrium lines with meteoric waters, which means that they were also formed under supergene conditions as suggested by Decrée et al. (2008b). Such high $\delta^{18}O$ values are unusual and might indicate that the Tamra white clays (and some goethites) are not exclusively formed by weathering processes in the presence of pure meteoric water. They could have crystallized either i) in the presence of highly evaporated meteoric waters, and/or ii) from waters that have previously intensive interactions with the country rocks at higher temperatures or even with magmatic fluids.

The first hypothesis (i) is deduced by the large variation recorded in the kaolinite and halloysite δD values (Fig. 6a) that could be attributed to meteoric waters that have experienced evaporation before their circulation within the bedrock. Evaporation processes affecting superficial waters would also have an effect on the isotopic composition: the heavier isotopes of oxygen and hydrogen are both favored in the residual meteoric fluid, leading to increasing and variable $\delta^{18}O$ and δD values (e.g., Bechtel et al., 1999). Such evaporation effect on the stable isotopes needs to be moderate with the paleoclimatic conditions that occurred during the deposition and the ore formation/enrichment of the Tamra succession. Late Miocene sediments recorded a change from a dry to a wet climate in North Africa, even more humid than today. The dry Tortonian climate changed to humid conditions (known as the

"Zeit Wet Phase") extending into the uppermost Tortonian and the lowermost Pliocene. Afterward, North Africa experienced a prolonged wet period during the Messinian, which is related to the interaction of Asian monsoon and the low stand of the Mediterranean Sea. The association of deserts and monsoons explains why the Mediterranean basin could be subject to desiccation (e.g. Messinian Salinity Crisis) while the areas in the south were receiving abundant rainfall (deMenocal and Bloemendal, 1995; Griffin, 2002; Gladstone et al., 2007). The Pliocene and Pleistocene were subject to alternating dry and wet episodes that did not match the "Zeit Wet Phase" intensity and length (e.g., Griffin, 1999, 2002; Köhler et al., 2010). While the following evaporation effect is consistent with the arid or subdesertic climate (Suc et al., 1995), particularly considering the hydromorphic pedogenesis, which have occurred during the ferralitisation of the Tamra sediments (Decrée et al., 2008b), the δD values of kaolinite-halloysite and goethite-hematite are probably too low to consider this process alone. The ^2H isotope would indeed be favored, and provide higher δD values as it has been observed in the Bahloul Formation (Fig. 6a; Bechtel et al., 1999). As this is not the case, the following O-isotope exchange model between hydrothermal/magmatic fluids with the basement rocks (ii) could be a better interpretation.

$\delta^{18}O$ and δD values of the kaolinite-halloysite samples also have a large range of values consistent with an input of heavy oxygen during their formation or during subsequent alteration. In this second hypothesis (ii), fluids with higher ^{18}O content compared to pure meteoric waters have contributed to the high $\delta^{18}O$ values measured for some samples relative to values recorded in kaolinites worldwide (Sheppard and Gilg, 1996, gray areas in Fig. 6a). The high $\delta^{18}O$ values may be the result of fluid-rock interaction with the basement rocks and supported by a high heat gradient related to magmatic intrusions. The presence of high $\delta^{18}O$ carbonates in the underlying Cretaceous to Eocene marls and/or skarns facilitates a fluid buffering towards higher ^{18}O contents (Fig. 6c). This hypothesis suggests that these kaolinite-halloysite were formed after synsedimentary weathering/pedogenesis and/or were altered in the presence of deeper hydrothermal fluids derived a few hundred meters beneath the Tamra deposit (Figs. 8a and b). The latter has been enhanced by alteration of the carbonated substratum, which may also have led to the enrichment of the mineralizing fluid in ^{18}O, and to the crystallization of kaolinite-halloysite and/or destabilization of the previously formed clay assemblages in the Tamra section (Fig. 8a). The occurrence of hydrothermal halloysite has already been mentioned in previous works (Hilali et al., 1968; Minato et al., 1981; Spencer, 1991; Lorenzoni et al., 1995; Nicaise, 1998; Joussein et al., 2005). The origin of this hydrothermal fluid could be meteoric, but a contribution of saline fluids is also consistent with the presence of a
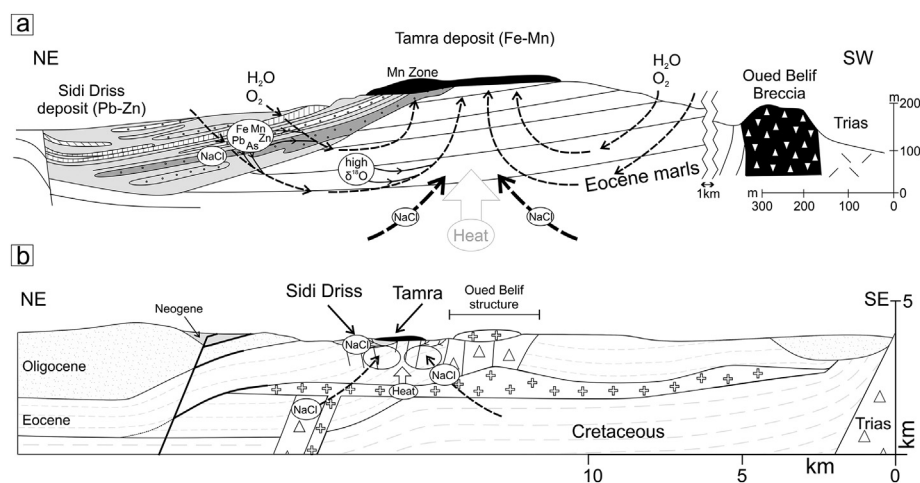
Fig. 8. Schematic cross section showing the Nefza area. a) Genetic model for the Tamra deposit hydrothermal enrichment and formation of the white clay levels. Mixing of meteoric fluids with saline hydrothermal solutions have led to alteration and transport of metals in the Tamra deposit. Leaching of the Pb-Zn Sidi Driss deposit has enriched mineralizing fluids in Fe, Mn, Pb, Zn, and As and subsequently crystallized late Mn-oxides in the Tamra section (Decrée et al., 2010). Fluid-rock interaction with underlying marls was responsible for heavy $\delta^{18}O$ related to carbonate phases, resulting in white clay formation in the Tamra deposit (adapted from Decrée et al., 2008b). b) Large scale model (adapted from Decrée et al., 2008a and references therein) showing the thermally driven circulation involved in the formation of SEDEX type Pb-Zn Sidi Driss ores. Such thermal activity probably persisted until current times as many thermal springs are still observed (Decrée et al., 2010). Note the contribution of deeper fluids originated from Triassic salt diapir, the heat flow related to the shallow magmatic sill underlying the Nefza area and normal faults acting as main drains for mineralization (Jallouli et al., 2003).

Triassic diapir beneath the surface of the Oued Belif structure a few hundred meters to the south of the Tamra deposit, and evaporite sediments in the underlying Sidi Driss basin (Figs. 2, 8a and b). The temperatures of the fluid responsible for the Pb-Zn ore in the underlying Sidi Driss deposit range from 80 °C (early mineral assemblage) to 150 °C (late mineral assemblage, Decrée et al., 2008a). However, these temperatures are probably not reached in the Tamra deposit because hydrothermal halloysite and kaolinite generally precipitate at low temperature (< 80 °C or < 61–110 °C, e.g.; Joussein et al., 2005). On the basis of the considered white clay samples and an estimated temperature of 80 °C, the modeling suggests a calculated isotope composition for a hot meteoric/magmatic fluid at 80 °C of −46 to −101‰ for δD, and 3.6 to 9.8‰ for $\delta^{18}O$ (Fig. 6a). Mixing the superficial O_2-rich meteoric waters with deeper saline hot brines could have triggered the formation of halloysite (and associated alteration minerals) in the Tamra deposit (Figs. 8a and b). The contribution of hydrothermal and meteoric fluids induced the crystallization of the typical supergene phases composed of hollandite, coronadite and chalcophanite, coexisting with kaolinite lenses at temperature less than those recorded in the Sidi Driss deposit. The timing of such process is poorly constrained but probably occurred during late diagenesis, coevally to hydrothermal enrichment described by Decrée et al. (2010; Fig. 5).

Considering the similarity between stable isotope compositions of the Tamra clays with those obtained by Bechtel et al. (1999) in the Bahloul Formation (Fig. 6a), and the presence of diapirism in the vicinity of both formations, saline fluids could have contributed to the transportation of base metals. Fluid inclusions of late calcite in the underlying Sidi Driss deposit corroborate this statement with 11.7 to 18.3 wt% NaCl (Decrée et al., 2008a). This high salinity, together with relatively low temperatures (< 150 °C), could have influenced the hydrogen and oxygen isotope composition of the fluid, as shown by experimental studies made by Truesdell (1974) and Horita et al. (1993). These authors showed that water composition can be more or less saline and does not directly influence the isotopic composition unless salinities are very high at such low temperatures of exchange. These features are in agreement with the conclusion learned from the Pb-Zn Bou Grine mine, where the origin of kaolinite is explained by the interaction of sedimentary pristine kaolinite with ^{18}O-rich hot saline brines (170–250 °C, 16–33 eq wt% NaCl; Charef and Sheppard, 1987; Bechtel et al., 1999).

Pb-Pb isotope results of the Fe and Pb ores define a clear trend ranging between the Nefza felsic magmatic rocks, and the carbonate substratum (Fig. 7). This suggests that the origin of Pb is not only related to felsic rocks but also to the substratum (Decrée et al., 2014). As a whole, the white clays plot on this trend, suggesting the same origin as the one for other Fe and Pb-Zn ores in the Nefza area (Decrée et al., 2008a, b). It would imply that i) mineralizing processes are quite similar to Sidi Driss and Tamra sequences and ii) mineralizing fluids from hydrothermal activity were related to magmatic bodies (Fig. 8b), passing through the carbonated substratum and forming Fe-oxides (hematite, goethite), Mn-oxides (hollandite, romanechite, strontiomelane, coronadite, Pb-Mn-oxides, chalcophanite), quartz and kaolinite-halloysite (Fig. 8a), and finally imposing their $\delta^{18}O$ and δD isotopic signatures. Such specific O and H isotopic compositions of the white clays can suggest the intervention of the same fluid, which was responsible for the white clay genesis and the late enrichment in Fe, Mn, Pb, Zn, and As (Fig. 5; *Stages 3 and 4*). Decrée et al. (2008a, b) pointed out the relation between the Tamra deposit and the underlying Sidi Driss deposit: the enrichment of Mn, Pb, Zn, Fe, and As in both deposits suggests that Fe-bearing fluids percolated through the Sidi Driss sulphide deposit before the enrichment of the Tamra ores. This late event indicates that hydrothermal activity has persisted in the Nefza mining district (Decrée et al., 2014) after the deposition and Fe-enrichment of the Tamra sediments. The enrichment in Pb-Zn of the co-genetic Mn-oxyhydroxide (chalcophanite, hollandite group minerals, romanechite) from the Tamra deposit is the result of reactivation of convection cells and leaching of hydrothermal fluid through the Sidi Driss deposit (Decrée et al., 2008a, b, 2010). Thermal anomalies have occurred since Late Serravallian-Tortonian times (Jallouli et al., 1996), the most striking example being the Messinian mafic magmatism (Decrée et al., 2013) and the current thermal springs (Zouiten, 1999).

The tectonic event favoring hydrothermal circulation at that time might be associated with the extensional opening of the late Miocene basins (Bouaziz et al., 2002) allowing the formation of the Tamra and Sidi Driss basins that are delineated by normal faults beneath and inside the Tamra deposit (Fig. 8b). Fluid flow was facilitated by the enhanced geothermal gradient, thanks to the intrusion of the shallow sill (Jallouli et al., 1996, 2003, Fig. 8b). In that context, structural discontinuities (thrust sheet boundaries, magmatic contacts and deformed plutons) could have served as main drains (Fig. 8b; Decrée et al., 2008a). This alteration process is not so clear as petrogenetic process related to hematite and goethite: the stable isotopes indicate that some of the goethite crystals/mineralizations were equilibrated with meteoric waters and plot along the 25 °C line, while others must have formed in the presence of the above-mentioned higher ^{18}O fluids (Fig. 6b). Therefore, the formation of Fe-oxides can be generated through synsedimentary weathering/pedogenesis, but also through hydrothermal fluid activities.

7. Conclusion

The high $\delta^{18}O$ values of the kaolinite-halloysite and goethite-hematite of the Fe-Mn Tamra deposit show that these latter minerals did not originate solely from an equilibrium state with pure meteoric waters. The most appropriate explanation for their relatively heavy isotopic values is a hydrothermal fluid-rock interaction of the meteoric fluid with the underlying carbonate rocks (marls and skarns), after deposition added to the synsedimentary weathering/pedogenesis of the Tamra succession. Such enrichment in the ^{18}O content of the fluid and clay minerals precipitating from the fluids is unusual and only observed in the Bahloul Formation hosting the Pb-Zn Bou Grine deposit. The occurrence of halloysite and kaolinite lenses in the Tamra deposit is assumed to be formed by a direct precipitation from hydrothermal fluids, or by a secondary fluid-mineral exchange during a post-depositional hydrothermal alteration of primary clays first formed during weathering. The structural discontinuities (mainly normal faults) may have supported the fluid migration. Pb isotopes of the white clays indicate that the source fluid could be influenced by felsic magmatism, when the carbonate bedrock is responsible for the enrichment of the fluid in $^{206}Pb/^{204}Pb$ and $^{207}Pb/^{204}Pb$ as it has been recorded in the halloysite-kaolinite and other mineralizations of the Nefza district. The close relation between Tamra ore deposition and the intrusion of a Triassic diapir into evaporites (also attributed to the Pb-Zn enrichment in the Bou Grine deposit) stimulates the occurrence of saline fluids that have facilitated the transportation of metals. The mineralizing fluid could be responsible for the ore enrichment in Mn, Fe, As, Pb, and Zn, and the formation of late Mn oxides in the Tamra deposit.

References

Badgasarian, G.P., 1972. Age radiométrique du volcanisme néogène du Nord de la Tunisie. Notes du Service Géologique de Tunisie 40, 79–85.
Batik, P., 1980. Carte Géologique de la Tunisie au 1:50000 - Hédil, feuille n°11.
Bauer, K.K., Vennemann, T.W., 2014. Analytical methods for the measurement of hydrogen isotope composition and water content in clay minerals by TC/EA. Chem. Geol. 363, 229–240.
Bechtel, A., Savin, S.M., Hoernes, S., 1999. Oxygen and hydrogen isotopic composition of clay minerals of the Bahloul Formation in the region of the Bou Grine zinc–lead ore deposit (Tunisia): evidence for fluid–rock interaction in the vicinity of salt dome cap rock. Chem. Geol. 156, 191–207.
Bellon, N., 1976. Séries magmatiques néogènes et quaternaires du pourtour de la Méditerranée occidentale comparées dans leur cadre géodynamique. In: Implications géodynamiques. Université Paris Sud, Orsay, pp. 363 (Unpublished Ph.D. thesis).
Ben Abdallah, R., 2013. Les phyllosilicates de la structure de l'Oued Bélif (Nefza, Tunisie septentrionale): minéralogie, géochimie et signification thermique (Unpublished Ph.D. thesis). Université de Carthage, Tunis, pp. 235.
Berthon, L., 1922. L'industrie minérale en Tunisie. Service des Mines de Tunisie, pp. 272.
Bouaziz, S., Barrier, E., Soussi, M., Turki, M.M., Zouari, H., 2002. Tectonic evolution of the northern African margin in Tunisia from paleostress data and sedimentary record. Tectonophysics 357, 227–253.
Bouhlel, S., Garnit, H., Bejaoui, J., Skaggs, S.A., 2013. Lead isotopes signatures of the MVT lead-zinc (± F) deposits across Central-North Tunisia: evidence for the heterogeneity in uranium component of the underlying source rocks. In: Mineral Deposit Research for a High-Tech World. Presented at the 12th Biennial SGA Meeting, Uppsala, pp. 612–615.
Bouzouada, R., 1992. Géologie, minéralogie et paragenèses des gites de fer du District des Nefza. Répartition des sulfures et des impuretés (Unpublished DEA). Université de Tunis, Tunis, pp. 77.
Brindley, G.W., Brown, G. (Eds.), 1980. Crystal Structures of Clay Minerals and their X-Ray Identification. Mineralogical Society of Great Britain and Ireland, Colchester and London, pp. 495.
Burollet, P.F., 1991. Structures and tectonics of Tunisia. Tectonophysics 195, 359–369.
Caillère, S., Hénin, S., Rautureau, M., 1982. Minéralogie des argiles, 2nd ed. Actualités scientifiques et agronomiques de l'I.N.R.A. Masson, Paris, New York, pp. 147.
Charef, A., Sheppard, S.M.F., 1987. Pb-Zn mineralization associated with diapirism: Fluid inclusion and stable isotope (H, C, O) evidence for the origin and evolution of the fluids at Fedj-el-Adoum, Tunisia. Chem. Geol. 61, 113–134.
Decrée, S., Marignac, C., De Putter, T., Deloule, E., Liégeois, J.-P., Demaiffe, D., 2008a. Pb–Zn mineralization in a Miocene regional extensional context: The case of the Sidi Driss and the Douahria ore deposits (Nefza mining district, northern Tunisia). Ore Geol. Rev. 34, 285–303.
Decrée, S., De Putter, T., Yans, J., Moussi, B., Recourt, P., Jamoussi, F., Bruyère, D., Dupuis, C., 2008b. Iron mineralisation in Mio-Pliocene sediments of the Tamra iron mine (Nefza mining district, Tunisia): mixed influence of pedogenesis and hydrothermal alteration. Ore Geol. Rev. 33, 397–410.
Decrée, S., Ruffet, G., Putter, T.D., Baele, J.-M., Recourt, P., Jamoussi, F., Yans, J., 2010. Mn oxides as efficient traps for metal pollutants in a polyphase low-temperature Pliocene environment: A case study in the Tamra iron mine, Nefza mining district, Tunisia. J. Afr. Earth Sci. 57, 249–261.
Decree, S., Marignac, C., De Putter, T., Yans, J., Clauer, N., Dermech, M., Aloui, K., Baele, J.-M., 2013. The Oued Belif Hematite-Rich Breccia: a miocene iron oxide Cu-Au-(U-REE) deposit in the Nefza Mining District, Tunisia. Econ. Geol. 108, 1425–1457.
Decrée, S., Marignac, C., Liégeois, J.-P., Yans, J., Ben Abdallah, R., Demaiffe, D., 2014. Miocene magmatic evolution in the Nefza district (Northern Tunisia) and its relationship with the genesis of polymetallic mineralizations. Lithos 192–195, 240–258.
Decrée, S., Marignac, C., Abidi, R., Jemmali, N., Deloule, E., Souissi, F., 2016. Tectonomagmatic Context of Sedex Pb–Zn and Polymetallic Ore Deposits of the Nappe Zone Northern Tunisia, and Comparisons with MVT Deposits in the Region. In: Bouabdellah, M., Slack, J.F. (Eds.), Mineral Deposits of North Africa. Springer International Publishing, Cham, pp. 497–525.
Dekoninck, A., Bernard, A., Barbarand, J., Saint-Bezar, B., Missenard, Y., Lepretre, R., Saddiqi, O., Yans, J., 2016a. Detailed mineralogy and petrology of manganese oxyhydroxide deposits of the Imini district (Morocco). Mineral. Deposita 51, 13–23.
Dekoninck, A., Leprêtre, R., Saddiqi, O., Barbarand, J., Yans, J., 2016b. The High-Grade Imini Manganese District—Karst-Hosted Deposits of Mn Oxides and Oxyhydroxides. In: Bouabdellah, M., Slack, J.F. (Eds.), Mineral Deposits of North Africa. Springer International Publishing, Cham, pp. 575–594.
deMenocal, P.B., Bloemendal, J., 1995. Plio-Pleistocene climatic variability in subtropical Africa and the paleoenvironment of Hominid evolution: A combined data-model approach. In: Vrba, E.S., Denton, G.H., Partridge, T.C., Burckle, L.H. (Eds.), Paleoclimate and Evolution, with Emphasis on Human Origins. Yale University Press, New Haven, pp. 262–288.
Dermech, M.-N., 1990. Le complexe de l'Oued Bélif - Sidi Driss (Tunisie septentrionale). Hydrothermalisme et métallogénie (Unpublished Ph.D. thesis). Université Pierre et Marie Curie - Paris VI, Paris, pp. 336.
Faul, H., Foland, K., 1980. L'âge des rhyodacites de Nefza-Sedjenane. Notes du Service Géologique de Tunisie. Travaux de Géologie Tunisienne 14, 47–49.
Galer, S.J.G., Abouchami, W., 1998. Practical Application of Lead Triple Spiking for Correction of Instrumental Mass Discrimination. Mineral. Mag. 62A, 491–492.
Garlick, G.D., 1966. Oxygen isotope fractionation in igneous rocks. Earth Planet. Sci. Lett. 1, 361–368.
Gharbi, M., 1977. Etude des minéralisations mercurifères de l'accident Ghardimaou-Cap Serrat (Tunisie du Nord-Ouest) (Unpublished Master thesis). Ecole Nationale Supérieure de Géologie Appliquée et de Prospection Minière de Nancy, Nancy, pp. 131.
Girard, J.P., Fouillac, A.M., 1995. Oxygen and hydrogen isotope geochemistry of clays: examples of application to diagenetic and geothermal environments. Bull. Centre Rec. Explor.-Production Elf Aquitaine 19, 167–195.
Gladstone, R., Flecker, R., Valdes, P., Lunt, D., Markwick, P., 2007. The Mediterranean hydrologic budget from a Late Miocene global climate simulation. Palaeogeogr. Palaeocl. 251, 254–267.
Gottis, C., Sainfeld, P., 1952. Les gîtes métallifères tunisiens. In: Monographie Régionales, 2. Presented at the 19ème Congrès Géologique International, Tunisie, pp. 104.
Griffin, D.L., 1999. The late Miocene climate of northeastern Africa: unravelling the signals in the sedimentary succession. J. Geol. Soc. Lond. 156, 817–826.
Griffin, D.L., 2002. Aridity and humidity: two aspects of the late Miocene climate of North Africa and the Mediterranean. Palaeogeogr. Palaeocl. 182, 65–91.
Hilali, E.A., Nataf, M., Ortelli, L., 1968. Les gites de kaolin du Maroc. In: Proceedings of Symposium I, Kaolin Deposits in the World, B Overseas Countries. Presented at the 23rd International Geological Congress, Prague, pp. 55–59.
Hoefs, J. (Ed.), 2009. Stable isotope geochemistry, Sixth edition. Springer, Berlin, pp. 285.
Holtzapffel, T. (Ed.), 1985. Les minéraux argileux: préparation, analyse diffractométrique et détermination. 12. Société Géologique du Nord, Villeneuve d'Ascq, pp. 130.

Horita, J., Wesolowski, D.J., Cole, D.R., 1993. The activity-composition relationship of oxygen and hydrogen isotopes in aqueous salt solutions: I. Vapor-liquid water equilibration of single salt solutions from 50 to 100 °C. Geochim. Cosmochim. Ac. 57, 2797–2817.

Jallouli, C., Inoubli, M.H., Albouy, Y.Y., 1996. Le corps igné de Nefza (Tunisie septentrionale): caractéristiques géophysiques et discussion du mécanisme de sa mise en place. Notes du Service Géologique de Tunisie, pp. 109–123.

Jallouli, C., Mickus, K., Turki, M.M., Rihane, C., 2003. Gravity and aeromagnetic constraints on the extent of Cenozoic volcanic rocks within the Nefza–Tabarka region, northwestern Tunisia. J. Volcanol. Geoth. Res. 122, 51–68.

Joussein, E., Petit, S., Churchman, J., Theng, B., Righi, D., Delvaux, B., 2005. Halloysite clay minerals – a review. Clay Miner. 40, 383–426.

Köhler, C.M., Heslop, D., Krijgsman, W., Dekkers, M.J., 2010. Late Miocene paleoenvironmental changes in North Africa and the Mediterranean recorded by geochemical proxies (Monte Gibliscemi section, Sicily). Palaeogeogr. Palaeocl. 285, 66–73.

Kohn, Matthew J., Valley, J.W., 1998a. Oxygen isotope geochemistry of the amphiboles: isotope effects of cation substitutions in minerals. Geochim. Cosmochim. Acta 62, 1947–1958.

Kohn, Matthew J., Valley, J.W., 1998b. Obtaining equilibrium oxygen isotope fractionations from rocks: theory and examples. Contrib. Mineral. Petrol. 132, 209–224.

Kohn, M.J., Valley, J.W., 1998c. Effects of cation substitutions in garnet and pyroxene on equilibrium oxygen isotope fractionations. J. Metamorph. Geol. 16, 625–639.

Lorenzoni, P., Mirabella, A., Bidini, D., Lulli, L., 1995. Soil genesis on trachytic and leucititic lavas of Cimini volcanic complex (Latium, Italy). Geoderma 68, 79–99.

Mauduit, F., 1978. Le volcanisme néogène de la Tunisie continentale (Unpublished Ph.D. thesis). Université Paris Sud, Orsay, pp. 157.

Maury, R.C., Fourcade, S., Coulon, C., El, Azzouzi, 'hammed, M., Bellon, H., Coutelle, A., Ouabadi, A., Semroud, B., Megartsi, M. 'hamed, Cotten, J., Belanteur, O., Louni-Hacini, A., Piqué, A., Capdevila, R., Hernandez, J., Réhault, J.-P., 2000. Post-collisional Neogene magmatism of the Mediterranean Maghreb margin: a consequence of slab breakoff. Comptes Rendus de l'Académie des Sciences - Series IIA – Earth Planet. Sc. Lett. 331, 159–173.

Minato, H., Kusukabe, H., Inoue, A., 1981. Alteration reactions of halloysite under hydrothermal conditions with acidic solutions. In: Proceedings of the 7th International Clay Conference. Presented at the International Clay Conference Development in Sedimentology, Bologna and Pavia, pp. 565–572.

Moussi, B., 2012. Mode de genèse et valorisation de quelques argiles de la région de Nefza-Sejnane (Tunisie septentrionale) (Unpublished Ph.D. thesis). Université de Carthage, Tunis, pp. 156.

Moussi, B., Medhioub, M., Hatira, N., Yans, J., Hajjaji, W., Rocha, F., Labrincha, J.A., Jamoussi, F., 2011. Identification and use of white clayey deposits from the area of Tamra (northern Tunisia) as ceramic raw materials. Clay Miner. 46, 165–175.

Negra, L., 1987. Pétrologie, minéralogie et géochimie des minéralisations et des roches encaissantes des bassins associés aux structures tectoniques et magmatiques de l'Oued Bélif et du Jebel Haddada (Nord des Nefza, Tunisie septentrionale) (Unpublished Ph.D. thesis). Université Paris Sud, Orsay, pp. 223.

Nicaise, D., 1998. L'halloysite des cryptokarsts de l'Entre-Sambre-et-Meuse (Belgique) : synthèse géologique, minéralogique et géochimique (Unpublished Ph.D. thesis). Université Paris Sud, Orsay, pp. 162.

Ould Bagga, M.A., Abdeljaouad, S., Mercier, E., 2006. The Tunissian "zone des nappes": a slightly inverted mesocenozoic continental margin (Taberka/Jendouba; northwestern Tunisia). B. Soc. Geol. Fr. 177, 145–154.

Piqué, A., Tricart, P., Guiraud, R., Laville, E., Bouaziz, S., Amrhar, M., Ait Ouali, R., 2002. The Mesozoic–Cenozoic Atlas belt (North Africa): an overview. Geodin. Acta 15, 185–208.

Renson, V., Coenaerts, J., Nys, K., Mattielli, N., Vanhaecke, F., Fagel, N., Claeys, P., 2011. Lead isotopic analysis for the identification of late bronze age pottery from Hala Sultan Tekke (Cyprus). Archaeometry 53, 37–57.

Rouvier, H., 1977. Géologie de l'extrême Nord-Tunisien: tectoniques et paléogéographie superposées à l'extrémité orientale de la chaîne Nord-Maghrebine (Unpublished Ph.D. thesis). Université Pierre et Marie Curie - Paris VI, Paris, pp. 215.

Rouvier, H., 1987. Carte Géologique de la Tunisie au 1:50000 - Nefza, feuille n°10.

Rouvier, H., 1994. Notice explicative de la carte géologique de la Tunisie au 1:50000 - Nefza, feuille n°10 (Notice). Office National des Mines, Direction de la Géologie, Tunis.

Rouvier, H., Perthuisot, V., Mansouri, A., 1985. Pb-Zn deposits and salt-bearing diapirs in Southern Europe and North Africa. Econ. Geol. 80, 666–687.

Savelli, C., 2002. Time–space distribution of magmatic activity in the western Mediterranean and peripheral orogens during the past 30 Ma (a stimulus to geodynamic considerations). J. Geodyn. 34, 99–126.

Savin, S.M., Epstein, S., 1970. The oxygen and hydrogen isotope geochemistry of clay minerals. Geochim. Cosmochim. Ac. 34, 25–42.

Savin, S.M., Hsieh, J.C., 1998. The hydrogen and oxygen isotope geochemistry of pedogenic clay minerals: principles and theoretical background. Geoderma 82, 227–253.

Savin, S.M., Lee, M., 1988. Isotopic studies of phyllosilicates. In: Hydrous Phyllosilicates (Exclusive of Micas). Mineralogical Society of America, pp. 189–223 Reviews in Mineralogy.

Sheppard, S.M.F., Gilg, H.A., 1996. Stable isotope geochemistry of clay minerals. Clay Miner. 31, 1–24.

Spencer, C., 1991. Mémento des roches et minéraux industriels: halloysite (No. R33266). BRGM, Orléans.

Spötl, C., Vennemann, T.W., 2003. Continuous-flow isotope ratio mass spectrometric analysis of carbonate minerals. Rapid Commun. Mass Sp. 17, 1004–1006.

Stefanov, S.H., Ouchev, A., 1972. Gisement plombo-zincifère de Sidi Driss (Rapport géologique avec estimation des réserves No. Unpublished Internal Report). Office National des Mines, Tunis.

Suc, J.P., Diniz, F., Leroy, S., Poumot, C., Bertini, A., Clet-Pellerin, M., Bessais, E., Zheng, Z., Dupont, L., Ferrier, J., 1995. Zanclean (~ Brunssumian) to early Piacenzian (~ early-middle Reuverian) climate from 4° to 54° north latitude (West Africa, West Europe and West Mediterranean areas). Med. Rijks Geol. Dienst. 43–56.

Taylor, H.P., 1968. The oxygen isotope geochemistry of igneous rocks. Contrib. Mineral. Petrol. 19, 1–71.

Truesdell, A.H., 1974. Oxygen isotope activities and concentrations in aqueous salt solutions at elevated temperatures: Consequences for isotope geochemistry. Earth Planet. Sci. Lett. 23, 387–396.

Vennemann, T.W., Morlok, A., von Engelhardt, W., Kyser, K., 2001. Stable isotope composition of impact glasses from the Nördlinger Ries impact crater, Germany. Geochim. Cosmochim. Ac. 65, 1325–1336.

Verhaert, M., Bernard, A., Saddiqi, O., Dekoninck, A., Essalhi, M., Yans, J., 2018. Mineralogy and Genesis of the Polymetallic and Polyphased Low Grade Fe-Mn-Cu Ore of Jbel Rhals Deposit (Eastern High Atlas, Morocco). Fortschr. Mineral. 8, 39.

Weis, D., Kieffer, B., Maerschalk, C., Barling, J., de Jong, J., Williams, G.A., Hanano, D., Pretorius, W., Mattielli, N., Scoates, J.S., Goolaerts, A., Friedman, R.M., Mahoney, J.B., 2006. High-precision isotopic characterization of USGS reference materials by TIMS and MC-ICP-MS: isotopic study of USGS reference materials. Geochem. Geophys. Geosy. 7, Q08006.

Yapp, C.J., 1990. Oxygen isotopes in iron (III) oxides: 1. Mineral-water fractionation factors. Chem. Geol. 85, 329–335.

Zouiten, S., 1999. Application de la géothermométrie chimique aux eaux des sources thermales du Nord de la Tunisie (Unpublished Ph.D. thesis). Univeristé de Tunis II, Tunis, pp. 197.